key components of our microscope are standard items in commercial product lines. This will make the technique easily accessible to a large community of materials scientists. The limited optical spectral resolution resulting from the large room-temperature zero phonon linewidth (FWHM = 30 cm^{-1} at $T = 300$ K) can be partly overcome by magnetic resonance. Such ODMR spectra contain a great variety of structural information; for example, on the distribution of other impurities around the center (*24*) or the local strain in the diamond lattice, as demonstrated here. More sophisticated ODMR experiments, including the use of ultrahigh magnetic field gradients (*28*) and ground-state nuclear magnetic resonance experiments, can be envisaged. The combination of these techniques with optical microscopy allows detailed material characterization at a local level that is otherwise masked by ensemble averaging.

REFERENCES AND NOTES

1. E. Betzig and R. J. Chichester, *Science* **262**, 1422 (1993).
2. X. S. Xie and R. C. Dunn, *ibid.* **265**, 361 (1994).
3. W. P. Ambrose, P. M. Goodwin, J. C. Martin, R. A. Keller, *ibid.*, p. 364.
4. W. E. Moemer, *et al., Phys. Rev. Lett.* **73**, 2764 (1994).
5. J. J. Macklin, J. K. Trautman, T. D. Harris, L. E. Brus, *Science* **272**, 255 (1996).
6. H. F. Hess, E. Betzig, T. D. Harris, L. N. Pfeiffer, K. W. West, *ibid.* **264**, 1740 (1994).
7. M. Nirmal, *et al.*, *Nature* **383**, 802 (1996).
8. J. E. Field, *The Properties of Diamond* (Academic Press, London, 1979).
9. J. I. Pankove and C. Qui, *Synthetic Diamond: Engineering CVD Science and Technology*, K. E. Spear and J. P. Dismukes, Eds. (Wiley, New York, 1994), pp. 401–418.
10. G. Davies and M. F. Hamer, *Proc. R. Soc. London Ser. A* **384**, 285 (1976).
11. R. T. Harley, M. J. Henderson, R. M. Macfarlane, *J. Phys. C: Solid State Phys.* **17**, L233 (1984).
12. N. R. S. Reddy, N. B. Manson, E. R. Krausz, *J. Lumin.* **38**, 46 (1987).
13. J. H. N. Loubser and J. A. van Wyk, *Rep. Prog. Phys.* **41**, 1201 (1978).
14. A. A. Kaplyanskii, *Optica Spectrosk.* **16**, 602 (1964).
15. G. Davies, *Properties and Growth of Diamond*, EMIS Data Review Series No. 9 (INSPEC, The Institution of Electrical Engineers, London, 1994).
16. A. T. Collins, M. F. Thomaz, M. I. B. Jorge, *J. Phys. C: Solid State Phys.* **16**, 2177 (1983).
17. The 514-nm line of an Ar^{+} ion laser was used for fluorescence excitation. An immersion oil objective (numerical aperture-1.3; magnification, ×100) collimated the excitation light and collected the sample fluorescence. A single photon-counting silicon avalanche photodiode was used as a detector. Stray light suppression was achieved with the use of a holographic notch and a red pass filter.
18. The saturated fluorescence intensity for a single center (detection efficiency 2%) is 1.7×10^{7} counts per second at an excitation intensity of 2.4 MW/cm^{2}.
19. J. Bernard, L. Fleury, H. Talon, M. Orrit, *J. Chem. Phys.* **98**, 850 (1993).
20. D. A. Redman, S. Brown, R. H. Sands, S. C. Rand, *Phys. Rev. Lett.* **67**, 3420 (1991).
21. D. Redman, S. Brown, S. C. Rand, *J. Opt. Soc. Am. B* **9**, 768 (1992).
22. S. P. McGlynn, T. Azumi, M. Kinoshita, *Molecular Spectroscopy of the Triplet State* (Prentice-Hall, Englewood Cliffs, NJ, 1970).
23. E. van Oort, thesis, University of Amsterdam (1990).
24. ______, P. Stroomer, M. Glasbeek, *Phys. Rev. B* **42**, 8605 (1990).
25. J. Köhler *et al.*, *Nature* **363**, 242 (1993).
26. J. Wrachtrup, C. von Borczyskowski, J. Bernard, M. Orrit, R. Brown, *ibid.*, p. 244.
27. J. Köhler, A. C. J. Brouwer, E. J. J. Groenen, J. Schmidt, *Science* **268**, 1457 (1995).
28. D. Rugar *et al.*, *ibid.* **264**, 1560 (1994).

29. We acknowledge stimulating discussions with R. Wannemacher, who pointed out the suitability of the N-V centers for single center detection. R. Pintaske supported us with the loan of a charge-coupled device camera. A. Boden and D. Bräunig from the Hahn Meitner Institute Berlin carried out the electron irradiation of the diamond samples. Support by the Deutsche Forschungsgemeinschaft through the Innovationskolleg "Methoden und Materialien für den Nanometerbereich" is gratefully acknowledged.

18 February 1997; accepted 14 April 1997

Creep Response of the Hayward Fault to Stress Changes Caused by the Loma Prieta Earthquake

James J. Lienkaemper,* Jon S. Galehouse, Robert W. Simpson

In 1996, an 18-millimeter creep event, the largest ever observed on the Hayward fault, occurred between surveys 63 days apart. This event marked the end of a period of severely reduced creep on the southern part of the fault that began after the 1989 Loma Prieta, California, earthquake. The reduction in creep was consistent with elastic models for earthquake-induced static stress changes on the Hayward fault. These data suggest that creep observations can indicate regional stress changes of about 1 bar or less.

Earthquake models generally assume that stress across plate tectonic boundaries increases steadily with time. However, large earthquakes can perturb the stress field acting on neighboring faults (*1*). We present evidence that the Loma Prieta earthquake affected the dynamics of creep on the nearby Hayward fault.

The probability of a magnitude (M) 7 or larger earthquake in the next 30 years on the Hayward fault is 45% (*2*), and it is thought to be the most hazardous fault zone in the San Francisco Bay region. The Hayward, a major branch of the San Andreas fault system, exhibits creep along at least 68 km of its <100 km length (Fig. 1). Creep rates over the past several decades vary along the fault from ~9 mm/year near the south end to ~3 mm/year in northern Oakland (*3*). The average rate for most of the fault is 4.8 mm/year (*3*). For decades before the 17 October 1989 Loma Prieta earthquake, creep rates at several monitoring sites, averaged over a few years, had gener-

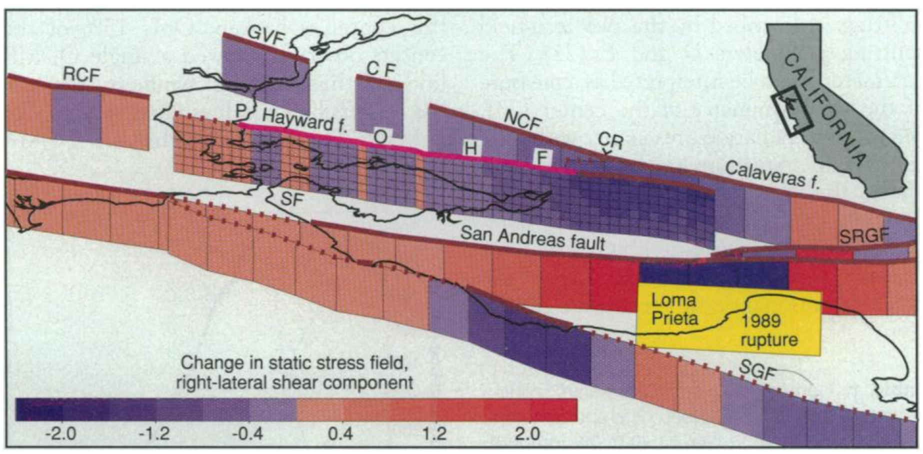

Fig. 1. Calculated static stress changes produced by Loma Prieta earthquake. Oblique view eastward of the San Francisco (SF) Bay region, California, shows the San Andreas fault system. Colored patches, mostly 10 km long by 13 km deep, show calculated changes in horizontal shear stress for each fault (*4, 5*). A red gradient indicates greater loading on a fault; blue indicates some relaxation of plate-tectonic driving stress. California map shows orientation of area in view, with the coastline in black for reference and active faults in brown. Faults are vertical, except the 1989 Loma Prieta earthquake rupture (*12*), shown in yellow, dips 70° SW. The 70-km-long, creeping Hayward fault trace is magenta; stress is computed at a grid size of 2 km. Locations: P, Point Pinole; O, Oakland; H, Hayward; F, Fremont; and CR, Calaveras Reservoir. Other faults: GVF, Green Valley; CF, Concord; NCF, Northern Calaveras; SRGF, Sargent; RCF, Rodgers Creek; and SGF, San Gregorio.

ally been steady (3). However, the M7.0 Loma Prieta earthquake, the largest in the region since the M7.8 earthquake in 1906, caused significant change in creep rate along most of the fault (3). Here, we present our observations of creep rate changes since the Loma Prieta earthquake, showing that these rate changes correlate well with calculated stress changes, both spatially (along strike; Fig. 2 and 3) and temporally by suppression of creep rates for a few years. Locations (for example, km 63) refer to the grid in Fig. 2A.

Using a three-dimensional elastic-dislocation model, we calculated expected changes in the regional stress field produced by the Loma Prieta earthquake (Fig. 1). This and similar models (4–6) imply that the Loma Prieta earthquake likely relaxed stress on the Hayward fault and acted to delay large earthquakes on the Hayward fault by a few years. Long-term effects are less certain as the calculated reduction in fault-normal stress may weaken the fault.

We measured creep precisely (survey error of <1 mm), using a first-order theodolite on three-point arrays (7). A few arrays were installed as early as 1966, and we recovered many lapsed older ones for this study. Since 1980, five arrays have been measured at bimonthly intervals. We added many new arrays since 1988, but survey intervals at these sites were irregular until mid-1992. The post–Loma Prieta creep rates shown in Fig. 2 were from 22 arrays where we had data for a 2.5- to 3-year interval following the 1989 earthquake. We used pre–Loma Prieta rates observed at the same locations as post–Loma Prieta array sites, except for one site where we used a rate from the weighted average curve.

Although the post–Loma Prieta reduction in creep is self-evident near the fault's south end, we also tested the more subtle reduction in creep to the north. Distinguishing small changes in creep rate at one site is difficult, especially for postearthquake rates, because they are short-term, and thus, more susceptible to nontectonic variance caused by such time-correlated effects as differential swelling and shrinking of the soils near the survey marks from rainy to dry season (8). Such seasonal noise in creep is equally likely to be right- or left-lateral in sense at a site. To reduce the effect of seasonal noise, we averaged rates along the entire fault except for the south end that crept ~9 mm/year. For the 17 sites with a 2.5- to 3-year-long sample of post–Loma Prieta creep, the fault crept at 4.79 ± 0.17 mm/year before the earthquake and 3.32 ± 0.47 mm/year after it. Despite the larger error in the data after Loma Prieta, this mean creep rate is distinctly lower than the long-term preevent rate.

J. J. Lienkaemper and R. W. Simpson, U.S. Geological Survey, 345 Middlefield Road, Mail Stop 977, Menlo Park, CA 94025, USA.
J. S. Galehouse, San Francisco State University, Department of Geosciences, 1600 Holloway Avenue, San Francisco, CA 94132, USA.

*To whom correspondence should be addressed.

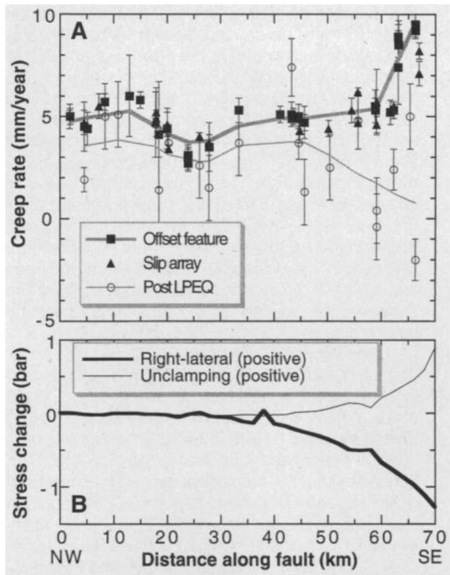

Fig. 2. Observed creep rates and calculated stress changes. Both upper and lower graphs are plotted versus distance along the Hayward fault southward from Point Pinole (P, Fig. 1). Errors (2σ) are for five bimonthly arrays; the rest show typical random walk error (8). (**A**) Rates before Loma Prieta earthquake (solid symbols) are indicated by: triangles, surveyed arrays; squares, surveyed offset cultural features—many reflecting decades of creep; Thick line, weighted average. Rates after the Loma Prieta earthquake (circles, post-LPEQ) until mid-1992; thin line, weighted average. (**B**) Stress changes expected from the Loma Prieta earthquake as shown in Fig. 1. Thick line indicates right-lateral (positive) horizontal shear component; thin line indicates fault normal stress changes, unclamping (positive). Hence, static stress changes on the fault are mostly left-lateral.

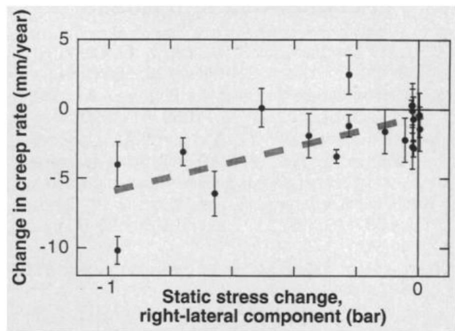

Fig. 3. Observed changes in creep rate versus calculated shear stress changes. Changes in creep rate are from data shown in Fig. 2; right-lateral is positive. Static stress changes are as shown in Figs. 1 and 2.

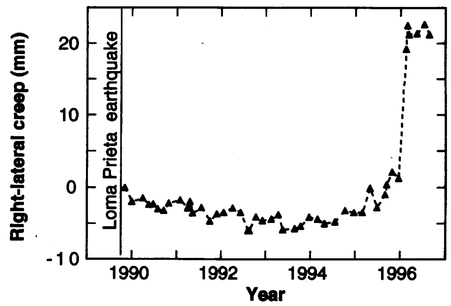

Fig. 4. Creep observed at an array near the south end of Hayward fault after the Loma Prieta earthquake. Creep rate at this location was ~9 mm/year (km 66.3) for decades before the earthquake, but was nearly zero thereafter until a large creep event in 1996.

The observed changes in creep correspond with calculated static stress changes (Fig. 3). The comparison suggests that the slowdown in creep was caused by the general drop in static stress expected for the fault. An alternative explanation is that a regional seasonal effect slowed creep, for example, the unusually strong drought condition that prevailed during 1986 to 1991. However, the data record is too brief to test the effect of prolonged drought on creep (3). Contrary to a drought explanation, we would not expect the greatest slowing of creep to be only along the southernmost part of the fault. The drought was no greater at the south end of the fault; however, much larger stress drops were expected there.

Long-term, dextral shear stress increases across the Hayward fault at ~0.15 bar/year (9). Thus, 6 to 7 years would be required for full recovery of creep rates at the south end of the fault after a stress drop of 1 bar. Near the south end of the fault (km 66.3), a pronounced recovery occurred in the form of the largest creep event ever measured on the fault (Fig. 4) (10). An 18-mm creep event occurred in the 63 days preceding a survey on 17 February 1996. Most of the fault had resumed creeping at rates at or near pre–Loma Prieta levels by 1994. A sudden resumption of fast creep in 1996, near the south end of the fault (km 65 to 67) (11), seems to indicate a full recovery from the stress relaxation expected from the Loma Prieta earthquake, and within a year or two of our model.

We conclude that a regional stress change of ~1 bar, small in the context of earthquake stressing cycles, seems to change creep rates enough to be detected. Thus, any future changes in stress large enough to significantly advance or retard expected recurrence times of major earthquakes should also change creep rates noticeably.

REFERENCES AND NOTES

1. R. W. Simpson, S. S. Schulz, L. D. Dietz, R. O. Burford, *Pure Appl. Geophys.* **126**, 665 (1988).
2. Working Group on California Earthquake Probabilities, *U.S. Geol. Surv. Circ.* **1053**, 51 (1990).
3. J. J. Lienkaemper, G. Borchardt, M. Lisowski [*J. Geophys. Res.* **96**, 18261 (1991)], being revised as J. J. Lienkaemper and J. S. Galehouse, in preparation; J. J. Lienkaemper, J. S. Galehouse, R. W. Simpson, *Eos* **73**, 119 (1992); ______, K. S. Breckenridge, *ibid.* **74**, 192 (1993).
4. P. A. Reasenberg and R. W. Simpson, *Science* **255**, 1687 (1992).
5. R. W. Simpson and P. A. Reasenberg, *U.S. Geol. Surv. Prof. Pap.* **1550-F**, 55 (1994).
6. J. S. Galehouse, *Geophys. Res. Lett.* **17**, 1219 (1990); *U.S. Geol. Surv. Prof. Pap.*, in press.
7. ______, B. D. Brown, B. Pierce, J. J. Thordsen, *Calif. Div. Mines Geol. Spec. Publ.* **62**, 239 (1982).
8. J. Langbein and H. Johnson, *J. Geophys. Res.* **102**, 591 (1997).
9. J. C. Savage and M. Lisowski, *ibid.* **98**, 787 (1993).
10. The previous largest event on the fault was 10 mm in 1983 during a 124-day interval at km 62. The date of the 18-mm event may be 9 February 1996, when a water main broke at km 65.9 on the fault. This 1996 event extended more than 1.7 km (from km 65.3 to 67.0), as shown on four arrays but less than 3.7 km, as limited by other data. We observed no triggered slip on the Hayward fault in 1989 except for 3 mm that showed on fresh cracks at km 66.3 (*3*).
11. Suddenness of resumption of fast creep from km 65 to 67 may be caused by two extremely rainy seasons following a drought. North of km 63, all sites had resumed pre–Loma Prieta rates by 1994. Two sites, km 63 and 64, resumed nearly normal rates during 1994. A creepmeter at km 63.6 resumed a 9 mm/year rate by late 1995 with no large event in early 1996. We note that a borehole strainmeter located 5 km northeast of the ~18-mm creep event recorded a strain event starting on 7 February 1996. These data are consistent with slip of 18 mm on a patch ~1 km in extent (M. Johnston, personal communication). Possibly, creep began steadily at depth months earlier, not slipping at the surface until induced by a water table raised by heavy rains.
12. M. Lisowski, W. H. Prescott, J. C. Savage, M. J. Johnston, *Geophys. Res. Lett.* **17**, 1437 (1990). Dislocation model parameters: 37 km in length; 316° strike, 70°SW dip; depth of 5 to 17.5 km; 1.66-m dextral slip; and 1.19-m reverse. Other models tested yield similar results for the Hayward fault (*4, 5*).

13. Funded by the U.S. Geological Survey National Earthquake Hazards Reduction Program (NEHRP) and San Francisco State University (NEHRP contract 1434-94-G2420). We thank many student assistants, especially C. Garrison, O. Graves, T. Hoyt, and F. McFarland; the governments of Fremont, Hayward, San Leandro, and Oakland; W. Hazelwood of the Bay Area Rapid Transit District; D. J. Russell; and two anonymous reviewers, W. Prescott and J. Langbein.

11 March 1997; accepted 5 May 1997

Single Polymer Dynamics in an Elongational Flow

Thomas T. Perkins, Douglas E. Smith, Steven Chu*

The stretching of individual polymers in a spatially homogeneous velocity gradient was observed through use of fluorescently labeled DNA molecules. The probability distribution of molecular extension was determined as a function of time and strain rate. Although some molecules reached steady state, the average extension did not, even after a ~300-fold distortion of the underlying fluid element. At the highest strain rates, distinct conformational shapes with differing dynamics were observed. There was considerable variation in the onset of stretching, and chains with a dumbbell shape stretched more rapidly than folded ones. As the strain rate was increased, chains did not deform with the fluid element. The steady-state extension can be described by a model consisting of two beads connected by a spring representing the entropic elasticity of a worm-like chain, but the average dynamics cannot.

The behavior of dilute polymers in elongational flow has been an outstanding problem in polymer science for several decades (*1, 2*). In elongational flows, a velocity gradient along the direction of flow can stretch polymers far from equilibrium. Extended polymers exert a force back on the solvent that leads to the important, non-Newtonian properties of dilute polymer solutions, such as viscosity enhancement and turbulent drag reduction.

A homogeneous elongational flow is defined by a linear velocity gradient along the direction of flow such that $\nu_y = \dot{\varepsilon}y$, where $\dot{\varepsilon} \equiv \partial\nu_y/\partial y$, the strain rate, is constant. Theory suggests that the onset of polymer stretching occurs at a critical velocity gradient or strain rate of $\dot{\varepsilon}_c$ of

$$\dot{\varepsilon}_c \approx \frac{0.5}{\tau_1} \tag{1}$$

where τ_1 is the longest relaxation time of the polymer (*3*). For $\dot{\varepsilon} < \dot{\varepsilon}_c$, the molecules are in a "coiled" state. But as $\dot{\varepsilon}$ is increased above $\dot{\varepsilon}_c$, the hydrodynamic force exerted across the polymer just exceeds the linear portion of the polymer's entropic elasticity, and the polymer stretches until its nonlinear elasticity limits the further extension of this "stretched" state. De Gennes predicted that this "coil-stretch transition" would be sharpened by an increase in the hydrodynamic drag of the stretched state relative to the drag of the coiled state (*1*).

In many types of elongational flows, such as flow through a pipette tip, the residency time t_{res} of the polymers in the velocity gradient is limited. To increase t_{res}, flows in which there is a stagnation point are often used. As molecular trajectories approach the stagnation point, t_{res} diverges. The classical techniques for inferring the degree of polymer deformation have been light scattering (*4, 5*) and birefringence (*6–9*). For example, Keller and Odell reported a rapid increase in the birefringence for $\dot{\varepsilon}$ above $\dot{\varepsilon}_c$ followed by a saturation (*6*). Such saturation was interpreted as an indication that the polymers had reached equilibrium in a highly extended state (*10*). Molecular weight analysis showed some chains are fractured in half, further supporting the hypothesis that the polymers reached full extension (*8, 11*). However, light-scattering experiments imply deformations of only two to four times the equilibrium size (*4, 5*). But, these "bulk" measurements average over a macroscopic number of molecules with a broad range of t_{res}. Moreover, only recent experiments have been dilute enough to prevent the polymers from altering the flow field (*9*).

Many rheological effects also remain unexplained. James and Saringer measured a pressure drop in a converging flow that was significantly greater than that predicted by simple models (*12*). Recently, Tirtaatmadja and Sridhar measured extensional viscosities η_E in filament stretching experiments that were several thousand times greater than the shear viscosities (*13*). At large deformations, η_E saturated, suggesting again that the polymers were fully extended. However, the measured stress was significantly lower than expected for fully extended polymers, implying that full extension had not actually been achieved (*14*). Also, the stress relaxation in such experiments contained both a strain-rate independent "elastic" and a strain-rate dependent "dissipative" component. The molecular origin of the dissipative component is uncertain (*15*). Examples such as these indicate that, even after a tremendous amount of study, the deformation of polymers in elongational flows is still poorly understood (*14, 16*).

We report the direct visualization of individual polymers in an elongational flow. The conformation and extension of each molecule was measured as a function of $\dot{\varepsilon}$ and t_{res}, thereby eliminating the ambiguities in conformation and t_{res}. We further eliminated polymer-polymer interactions and polymer-induced alterations of the flow field by working with single isolated molecules. The inherent uniformity

Department of Physics, Stanford University, Stanford, CA 94305, USA.

*To whom correspondence should be addressed. E-mail: schu@leland.stanford.edu